Bulletin of the Seismological Society of America, Vol. 106, No. 2, pp. 499–511, April 2016, doi: 10.1785/0120150158

Joint Determination of Event Epicenter and Magnitude from Seismic Intensities

by Seongjun Park and Tae-Kyung Hong

Abstract Characteristic features of seismicity with long recurrence intervals can be deduced from analysis of historical earthquake records that inherently suffer from uncertainty in the event locations and magnitudes. A novel method to determine the event epicenters and magnitudes jointly from seismic intensities is proposed. The probability for a set of event epicenter and magnitude is assessed by accounting the fitness between the observed and reference seismic intensities, spatial-occurrence probability based on seismicity density distribution, and temporal-occurrence probability from the Gutenberg–Richter magnitude–frequency relationship. A set of event epicenter and magnitude yielding the peak probability is chosen. The validity of the method is tested for both synthetic and instrumental seismic-intensity data, confirming high accuracy. The method is applied effectively to historical events with written seismic damage records. It is found that the errors generally decrease with increasing number and azimuthal coverage of seismic-intensity data, and increase with epicentral distances. The method appears to be promising for historical earthquakes of which source properties are poorly known. The method is applicable for assessment of the properties of long-period seismicity, which is crucial for assessment of potential seismic hazards.

Introduction

Large events naturally have long recurrence intervals (Shimazaki and Nakata, 1980; Schwartz and Coppersmith, 1984; Pearthree and Calvo, 1987). It is crucial to consider long-time seismicity for proper assessment of potential seismic hazards (e.g., Kawasumi, 1951; Frankel, 1995; McGuire, 1995; Stirling *et al.*, 1998; Stirling and Petersen, 2006; Miyazawa and Mori, 2009).

Instrumental seismicity records are only available for a short time (since the introduction of modern seismometers), which is insufficient for representation of seismicity of long recurrence intervals. The preinstrumental seismicity should be reflected for proper seismic-hazard analysis. Seismic damages by historical earthquakes are described in historical literatures. The seismic damages can be converted to seismic intensities. The historical earthquake records may be useful to assess the long-term seismicity. However, they have inherent limitation in source parameters including event locations and magnitudes.

Seismic damage is generally proportional to the event magnitude and decreases with distance (Howell and Schultz, 1975). Conventionally, the epicenters of historical earthquakes are determined to be the locations of the largest damages or the central locations of equidamage regions (e.g., Degasperi *et al.*, 1991; Wang, 2004; Lee and Yang, 2006; Seo *et al.*, 2010). The event magnitudes are estimated from empirical relationships between seismic intensities and magnitudes.

When a number of seismic intensities are available over a wide region, an isoseismal map can be used for the determination of the event epicenter (e.g., Sibol *et al.*, 1987; Levret *et al.*, 1994; Albarello *et al.*, 1995; Termini *et al.*, 2005). In this case, the magnitude is estimated from the size of isoseismal area. The accuracy of the estimated epicenters and magnitudes is highly dependent on the spatial coverage of observed seismic damages in such conventional methods. Also, the event magnitude interlocks with the event location.

Recently, Houng and Hong (2013) proposed a probabilistic approach to determine the epicenters of historical earthquakes using the instrumental seismicity densities, allowing analysis of offshore events as well as inland events. This probabilistic approach is useful to determine the stochastic properties of overall historical seismicity. However, the approach inherently suffers from nonunique determination of source parameters of particular events.

In this study, we propose a novel probabilistic method to determine the source parameters of historical events uniquely from seismic intensities using the instrumental seismicity density and the instrumental Gutenberg–Richter magnitude–frequency relationship. The proposed method is verified by synthetic tests and instrumental-event data. The method is finally applied to historical seismic-intensity data for the determination of unknown source parameters of historical events.

Theory

Reference Seismic-Intensity Attenuation Curve

The seismic damage is proportional to seismic energy (magnitude) radiated from the sources and decreases with distance (e.g., Bakun and Wentworth, 1997; Sørensen *et al.*, 2009; Szeliga *et al.*, 2010). In addition, the seismic damage is controlled by source radiation pattern, seismic attenuation, site amplification, and source strength that are associated with medium properties and tectonic environment (e.g., Howell and Schultz, 1975; Tilford *et al.*, 1985; Sokolov, 2002). It is observed that the seismic intensities attenuate differently with distance by region (e.g., Howell and Schultz, 1975; Bakun and Wentworth, 1997; Musson, 2005; Szeliga *et al.*, 2010).

The reference seismic-intensity variation can be expressed as a function of magnitude and distance, which is given by

$$I^{\mathrm{ref}}(m,l,h) = c + \alpha m - \beta \ln(l^2 + h^2) - \gamma\sqrt{l^2 + h^2} \quad (1)$$

(e.g., Musson, 2005; Szeliga *et al.*, 2010), in which I^{ref} is the seismic intensity in modified Mercalli intensity (MMI) scale, m is the magnitude, l is the epicentral distance in kilometers, h is the focal depth in kilometers, and c, α, β, and γ are calibration constants for source strength and seismic-intensity attenuation rate associated with geometric spreading, anelastic absorption, and scattering (Howell and Schultz, 1975).

Gutenberg–Richter Magnitude–Frequency Relationship

It is known that natural seismicity satisfies the Gutenberg–Richter magnitude–frequency relationship:

$$\log(N_m) = a - bm \quad (2)$$

(Gutenberg and Richter, 1954), in which N_m is the number of events with magnitudes greater than, equal to, or larger than m, and a and b are constants. The relationship presents that the earthquake recurrence interval increases with the magnitude. Constant a calibrates the number of earthquakes, whereas constant b controls the relative occurrence frequency for magnitudes. The constants a and b are region dependent (e.g., Aki, 1965; Tinti and Mulargia, 1987; Seo *et al.*, 2010; Hong, Lee, and Houng, 2015; Hong, Park, and Houng, 2015). The constants a and b are determined for earthquake catalogs ensuring the completeness (e.g., Aki, 1965; Wiemer and Wyss, 2000).

Seismicity Density Distribution

Seismic activity is controlled by the stress field and medium properties, constructing characteristic distribution of seismicity. Large earthquakes generally occur in high seismicity regions, following the general seismicity density distribution (e.g., Kossobokov *et al.*, 2001; Houng and Hong, 2013). Houng and Hong (2013) presented a high correlation between current seismicity density distribution and past large earthquakes in California. The seismicity density distribution can be useful to constrain possible event locations.

The seismicity density function is calculated by smoothing the spatial densities of seismicity with magnitudes greater than the minimum magnitude ensuring the completeness of earthquake catalog. The seismicity density at the ith cell D_i is given by

$$D_i = \sum_{j=1}^{N_c}\left[n_j \times \exp\left(\frac{-l_{ij}^2}{2\sigma_c^2}\right)\right] \Big/ \sum_{j=1}^{N_c}\left[\exp\left(\frac{-l_{ij}^2}{2\sigma_c^2}\right)\right] \quad (3)$$

(Houng and Hong, 2013), in which N_c is the number of cells discretizing the medium, n_j ($j = 1, 2, \ldots, N_c$) is the number of earthquakes in the jth cell, l_{ij} is the epicentral distance between the ith cell and the jth cell, and σ_c controls the decay rate of the Gaussian function that is set to be 20 km (Houng and Hong, 2013).

Probabilistic Determination of Source Parameters

Observed seismic intensities are expected to follow the reference seismic-intensity attenuation curve that is a function of distance and magnitude. This feature allows us to constrain the event location and magnitude from the fitness between the observed seismic intensities and the reference seismic-intensity attenuation curve. The magnitude can be additionally constrained by the Gutenberg–Richter relationship that controls the relative occurrence chances among events with different magnitudes. Events with larger magnitudes have lower chances of occurrence. Also, the spatial distribution of seismicity densities provides relative probability as event location.

A posterior probability function is defined to be a product of likelihood function and prior probability function (e.g., Vaseghi, 2001). The likelihood function of event location and magnitude is determined using the fitness between the reference and observed seismic intensities. The magnitude-dependent event occurrence rate is used as a prior probability function of event magnitude. Also, the seismicity density is used as a prior probability function of event location. The posterior probability function is a multiplication of the likelihood function for seismic-intensity curve fitness and the prior probability functions of event magnitude and location.

The posterior probability function $P_{i,m}$ as a function of location i and magnitude m is given by

$$P_{i,m} = L_{i,m} \times F_m \times C_i, \quad (4)$$

in which $L_{i,m}$ is a function estimating the fitness between the reference and observed seismic intensities, function F_m accounts for the relative occurrence chance of earthquake with magnitude m, and function C_i presents the seismicity density at the ith cell.

The differences between the reference and observed seismic intensities are expected to follow a Gaussian distribution (e.g., Gómez Capera, 2006). The seismic-intensity fitness function $L_{i,m}$ is represented to be

$$L_{i,m} = \frac{E_{i,m}}{E_{\max}}, \tag{5}$$

in which $E_{i,m}$ is the fitness function, and $E_{\max}$ is the peak fitness value for all discrete sets of i and m ($i = 1, 2, \ldots, N_c$, $m = M_{\min}, \ldots, M_{\max}$) in which $M_{\min}$ and $M_{\max}$ are the minimum and maximum magnitudes. Function $E_{i,m}$ is given by

$$E_{i,m} = \prod_{j=1}^{n} \exp\left[-\frac{\{I^{\mathrm{ref}}(m, l_{ij}, h) - I_j^{\mathrm{obs}}\}^2}{2\sigma_l^2}\right], \tag{6}$$

in which n is the number of observed seismic intensities, $I^{\mathrm{ref}}(m, l_{ij}, h)$ is the reference seismic intensity at site j for an event with magnitude m occurring at the ith cell, l_{ij} is the epicentral distance between cell i and site j, h is the focal depth, I_j^{obs} is the observed seismic intensity at site j, and σ_l is the standard deviation of the Gaussian function.

The relative earthquake occurrence frequency of an event with magnitude m, F_m, is determined according to the Gutenberg–Richter magnitude–frequency relationship:

$$F_m = \frac{10^{-bm}}{10^{-bM_{\min}}}, \tag{7}$$

in which b is the Gutenberg–Richter constant. The normalized seismicity density at cell i, C_i, is given by

$$C_i = \frac{D_i}{D_{\max}} \tag{8}$$

(Houng and Hong, 2013), in which D_i is a smoothed seismicity density for cell i that is given in equation (3), and $D_{\max}$ is the peak seismicity density for all cells ($i = 1, 2, \ldots, N_c$).

Equation (4) can be restated to be

$$P_{i,m} = \exp\left[-\frac{\sum_{j=1}^{n}\{I^{\mathrm{ref}}(m, l_{ij}, h) - I_j^{\mathrm{obs}}\}^2 + 2\ln(10)\sigma_l^2 bm}{2\sigma_l^2}\right] \times G_i, \tag{9}$$

in which G_i is a composite magnitude-independent function:

$$G_i = \frac{D_i}{10^{-bM_{\min}} \times E_{\max} \times D_{\max}}. \tag{10}$$

Here the event magnitude M_i yielding the peak posterior probability for event location i satisfies

$$\frac{\partial P_{i,m}}{\partial m}\Big|_{m=M_i} = 0, \tag{11}$$

which gives

$$\frac{\partial}{\partial m}\left[\sum_{j=1}^{n}\{I^{\mathrm{ref}}(m, l_{ij}, h) - I_j^{\mathrm{obs}}\}^2 + 2\ln(10)\sigma_l^2 bm\right]\Big|_{m=M_i} = 0. \tag{12}$$

If I^{ref} is expressed as equation (1), M_i satisfying equation (12) can be calculated by

$$M_i = \frac{\sum_{j=1}^{n}\left[I_j^{\mathrm{obs}} - c + \beta\ln(l_{ij}^2 + h^2) + \gamma\sqrt{l_{ij}^2 + h^2}\right]}{n \times \alpha} - \frac{\ln(10) \times b \times \sigma_l^2}{n \times \alpha^2}. \tag{13}$$

The location i yielding the peak posterior probability with magnitude of M_i is selected as the optimal event location. Here, the event magnitude is determined subsequently. However, it is noteworthy that the likelihood function $L_{i,m}$ varies according to the prior probability function F_m. Thus, the magnitude M_i is expected to be deviated from the true optimal value, M_i^{op}:

$$M_i^{\mathrm{op}} = M_i - \delta M, \tag{14}$$

in which δM is the magnitude difference that is defined to be

$$\delta M = M_i^{\mathrm{ex}}(M^{\mathrm{tr}}, i) - M^{\mathrm{tr}} \tag{15}$$

(Vaseghi, 2001), in which $M_i^{\mathrm{ex}}(M^{\mathrm{tr}}, i)$ is the expected magnitude estimate for an event with true magnitude of M^{tr} and epicenter of i. Here, from equation (13), M_i^{ex} can be calculated by

$$M_i^{\mathrm{ex}}(M^{\mathrm{tr}}, i) = \frac{\sum_{j=1}^{n}\left[I_j^{\mathrm{ex}}(M^{\mathrm{tr}}, i) - c + \beta\ln(l_{ij}^2 + h^2) + \gamma\sqrt{l_{ij}^2 + h^2}\right]}{n \times \alpha} - \frac{\ln(10) \times b \times \sigma_l^2}{n \times \alpha^2}, \tag{16}$$

in which $I_j^{\mathrm{ex}}(M^{\mathrm{tr}}, i)$ is the expected seismic-intensity estimate at site j for an event with magnitude M^{tr} and epicenter i. Also, the expected seismic-intensity estimate corresponds to $I^{\mathrm{ref}}(M^{\mathrm{tr}}, l_{ij}, h)$, yielding the magnitude difference, δM, to be

$$\delta M = -\frac{\ln(10) \times b \times \sigma_l^2}{n \times \alpha^2}. \tag{17}$$

Data and Seismicity Properties

The Korean Peninsula is a unique region with dense seismic monitoring networks and well-preserved historical earthquake records allowing us to test a new method for both instrumental

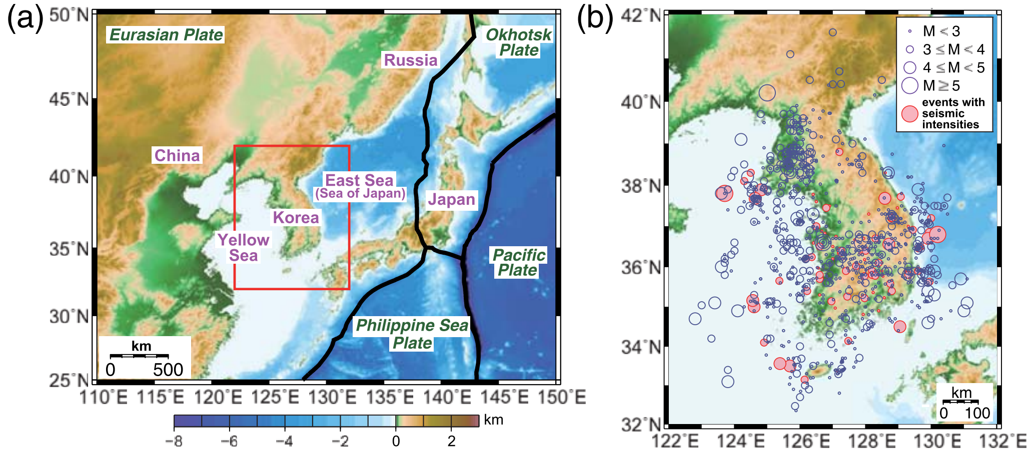

Figure 1. (a) Map of tectonic setting around the Korean Peninsula. The plate boundaries are marked with thick solid lines. The study area is marked with a rectangular box. (b) An enlarged map around the Korean Peninsula with seismicity during 1978–2013. The events with reported seismic intensities are marked with filled circles. The color version of this figure is available only in the electronic edition.

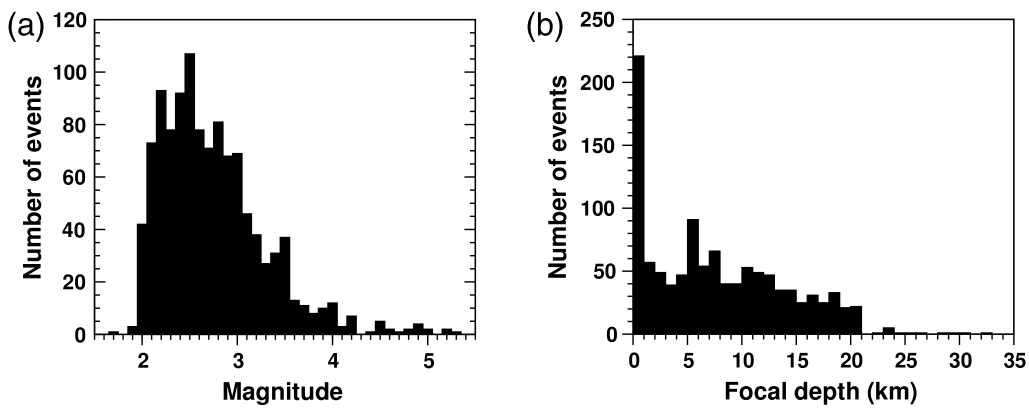

Figure 2. Distribution of (a) magnitudes and (b) focal depths of the instrumentally recorded earthquakes in Figure 1. The magnitudes range between 1.7 and 5.3. The focal depths of most events are less than 21 km. The average focal depth is 7.3 km.

and historical earthquake data. We analyze 1119 instrumentally recorded earthquakes during 1978–2013 of which source information is collected from the Korea Meteorological Administration (KMA) and the Korea Institute of Geoscience and Mineral Resources (KIGAM) (Fig. 1). The event magnitudes are M_L 1.7–5.3 (Fig. 2). The focal depths are shallower than 42 km, and the average focal depth is 7.3 km (Fig. 2).

Seismic-intensity data are available from the official seismicity reports of KMA and some previous studies. Seismic intensities for 55 earthquakes with magnitudes of 3.0 or larger during 2001–2013 are collected from the seismicity reports of KMA (2002, 2003, 2004, 2005, 2006, 2007, 2008, 2009, 2010, 2011, 2012b, 2013, 2014) (Fig. 1). The seismic intensities for the 20 January 2007 M_L 4.8 earthquake are additionally collected from Kyung *et al.* (2007). The number of collected seismic intensities is 353 that corresponds to ~6.4 per event on average. The seismic intensities range between I and VI in the MMI scale.

Historical seismic damage records were originally collected from historical literatures including Samguksagi, Koryosa, and Choseonwangjosillog. The seismic intensities for the historical seismic damages are available from previous studies (e.g., Lee and Yang, 2006; KMA, 2012a). The number of reported historical earthquakes is 2161.

The Korean Peninsula is located in the eastern margin of the Eurasian plate that is adjacent to the Pacific plate and Philippine sea plate (Fig. 1). The plate collision geometry constructs an east-northeast–west-southwest directional compression field in and around the Korean Peninsula (Choi *et al.*, 2012). The Korean Peninsula is located in a stable intraplate environment and is composed of complex geological and tectonic structures (Chough *et al.*, 2000; Hong and Choi, 2012).

The reference seismic-intensity attenuation function for the Korean Peninsula is given by

$$I^{\mathrm{ref}}(m,l,h) = -0.998 + 1.72m - 0.322\ln(l^2+h^2) - 0.00608\sqrt{l^2+h^2} \tag{18}$$

(Park and Hong, 2014). The differences between the observed seismic intensities and the reference seismic-intensity

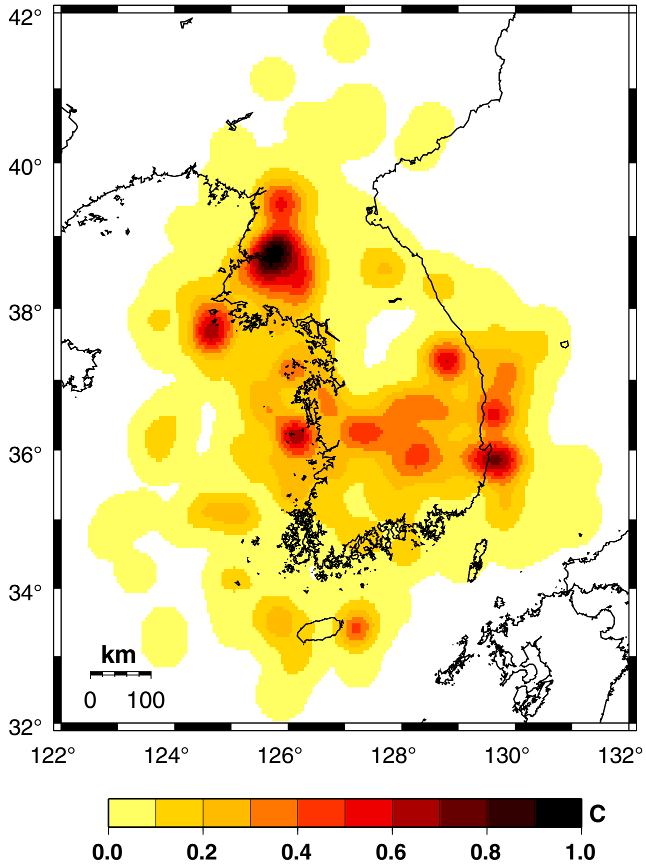

Figure 3. Seismicity densities of instrumentally recorded earthquakes around the Korean Peninsula. The seismicity densities are high in the northwestern and southern Korean Peninsula, and relatively low in the central and northeastern Korean Peninsula. The seismicity is high in the regions off the west and southeast coasts. The color version of this figure is available only in the electronic edition.

attenuation curve present a normal distribution with a standard deviation of 0.65 in MMI unit.

The threshold magnitude, $M_{\min}$, ensuring the completeness of event catalog is determined to be 2.5 (Hong, Lee, and Houng, 2015; Hong, Park, and Houng, 2015). Also, the Gutenberg–Richter b-value is found to be around 0.92 (Hong, Lee, and Houng, 2015; Hong, Park, and Houng, 2015). The seismic density distribution is obtained from instrumentally recorded data for the region in latitudes between 32° and 42° N and longitudes between 122° and 132° E that is discretized into cells with a uniform size of 0.05° × 0.05°. The number of cells N_c is 40,000. Earthquakes with magnitudes equal to or greater than the threshold magnitude ($M_{\min} = 2.5$) are analyzed. The seismicity densities are observed to be high in the northwestern and southern Korean Peninsula, and low in the central and northeastern Korean Peninsula (Fig. 3).

Validation Tests for Various Conditions

The azimuthal coverage, epicentral distances to stations, and number of observations are generally dependent on the physical and monitoring environment. The proposed method is tested with synthetic data for verification in various conditions. Synthetic data sets of seismic intensities for various configurations of observation positions are prepared. The observation points for each configuration are set to be placed evenly over the arc with a radius of the epicenter distance (Fig. 4). We consider the cases with the number of observation points of 1, 2, 3, 5, 10, and 20. Spatial distribution of observation points with azimuthal coverages of 10°, 30°, 60°, 120°, and 240° is considered. We consider epicentral distances of 10, 20, 50, 100, and 200 km for each case. We constitute 125 different configurations of observation positions from various combinations of azimuthal coverages, epicentral distances, and numbers of seismic intensities. The influences of azimuthal coverage, epicentral distance, and number of observations on the determination of magnitudes and epicenters are examined.

The event magnitude is set to be 5.0. The focal depth is set to be 7.3 km, considering the average focal depth of earthquakes in the Korean Peninsula. Synthetic seismic intensities are calculated from equation (18) with addition of Gaussian random errors of which standard deviation is set to be 0.65 in MMI unit, considering the residuals between the reference and observed seismic intensities (Park and Hong, 2014). The synthetic intensities are rounded off to be integers in MMI scale. We produce 100 synthetic seismic-intensity data sets for each observation configuration. A uniform seismicity density with the Gutenberg–Richter b-value of 0.92 is assumed over the medium. The medium is discretized into 1 km × 1 km cells. We search the locations and magnitudes of peak probabilities. The apparent deviation of magnitudes is corrected using equation (15).

The estimated locations and magnitudes are compared with input parameters (Fig. 5). It is found that the accuracy of estimated parameters generally increases with the number of seismic intensities (N_I). Also, the error of estimated parameters is proportional to the distance. We find that the errors of estimated parameters decrease with the central angle of arc. The errors reach zero in cases with central angles greater than 120°. The parameters are poorly estimated particularly with seismic-intensity data from stations on small azimuthal arcs in large distances.

Application to Synthetic Earthquakes

The proposed method is tested for imaginary earthquakes in the seismological environment of the Korean Peninsula. We consider earthquakes that are distributed randomly in the region with latitudes between 32° and 42° N and longitudes between 122° and 132° E. The actual instrumental seismicity density distribution over the peninsula is considered for the synthetic test. We consider imaginary seismic events with magnitudes equal to or greater than 3.0. The event magnitudes satisfying the Gutenberg–Richter magnitude–frequency relationship with b-value of 0.92 are selected randomly. The focal depth is set to be 7.3 km. The potential

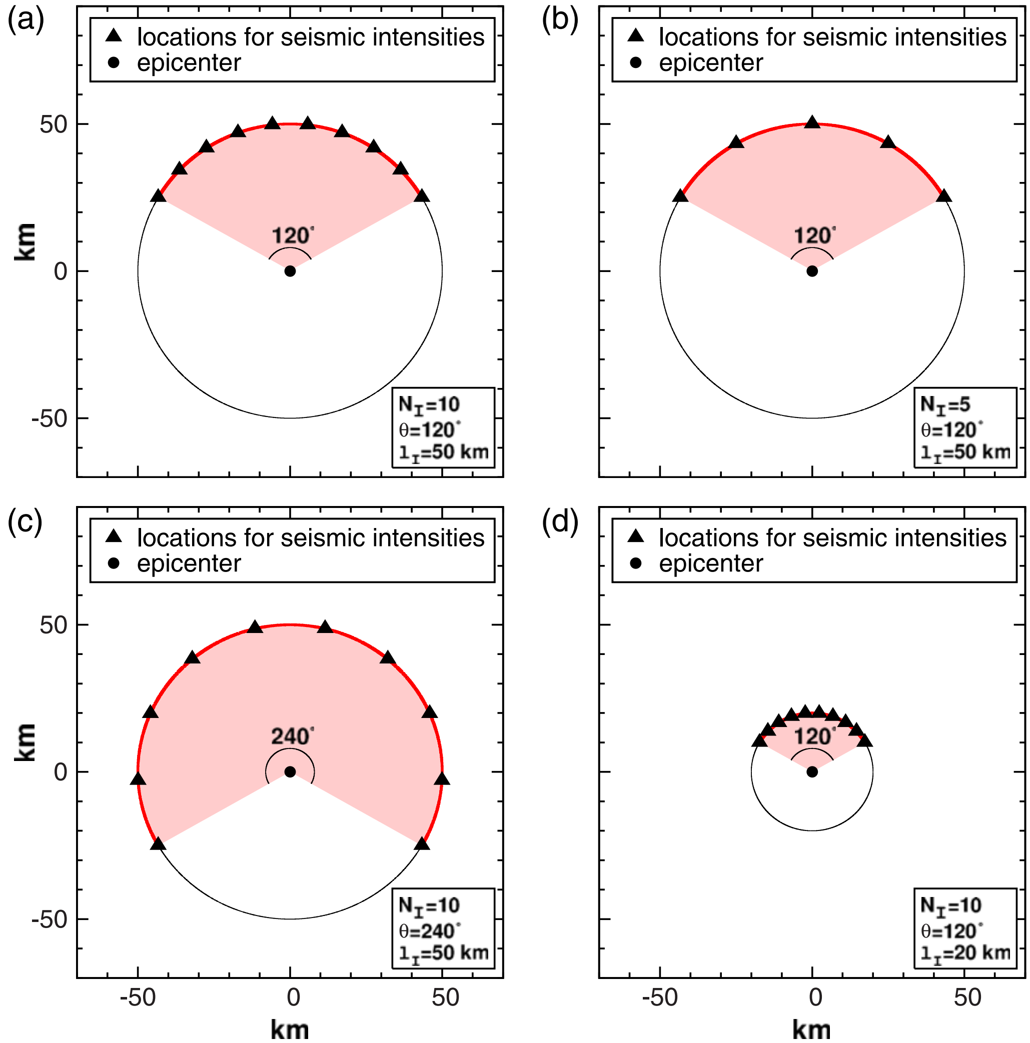

Figure 4. Examples of spatial configuration of seismic-intensity observation positions. (a) A case with 10 seismic-intensity data ($N_I = 10$) at azimuthal coverage of $\theta = 120°$ and epicentral distance of $l_I = 50$ km; (b) a case with $N_I = 5$, $\theta = 120°$, and $l_I = 50$ km; (c) a case with $N_I = 10$, $\theta = 240°$, and $l_I = 50$ km; and (d) a case with $N_I = 10$, $\theta = 120°$, and $l_I = 20$ km. The events are located in the centers of circles. The locations of seismic-intensity data (filled triangles) are placed evenly over the azimuthal ranges. The color version of this figure is available only in the electronic edition.

locations of stations are on the inland region at every 0.01° in longitude and latitude (Fig. 6).

We generate 1000 imaginary events of which epicenters and magnitudes are chosen, considering the seismicity density distribution and Gutenberg–Richter magnitude–frequency relationship. The synthetic seismic intensities are produced from the reference seismic-intensity attenuation curve. The observation points of seismic intensities are chosen randomly. The selection chance of observation point is designed to be inversely proportional to its epicentral distance with an idea that a near location generally has a bigger seismic damage than a far location. We compose the synthetic data sets with $1, 2, 3, \ldots, 19$, and 20 seismic intensities for each event. The seismic intensities are equal to or greater than MMI I.

The study region is discretized by $0.05° \times 0.05°$ cells. The probability of each discrete position is estimated. The location with the highest probability is determined to be the event epicenter. It is observed that the errors in event magnitudes and epicenters are highly dependent on the numbers of seismic intensities (Figs. 7, 8). The event magnitudes are generally underestimated when a single seismic-intensity observation is available. The average error in magnitude estimates for the inversions with single seismic intensities is −0.80 in magnitude unit, and the standard deviation is 0.64 in magnitude unit (Table 1).

On the other hand, the mean value and standard deviation of magnitude-estimate errors for inversions based on two seismic-intensity data are −0.26 and 0.49 in magnitude unit, respectively, presenting significantly increased accuracy compared with inversions based on single seismic-intensity data. The accuracy of event magnitude increases with the number of seismic-intensity data. It is observed that inversions with 4 or more seismic-intensity data produce reasonable magnitude estimates with mean errors less than or equal to 0.1 in magnitude unit.

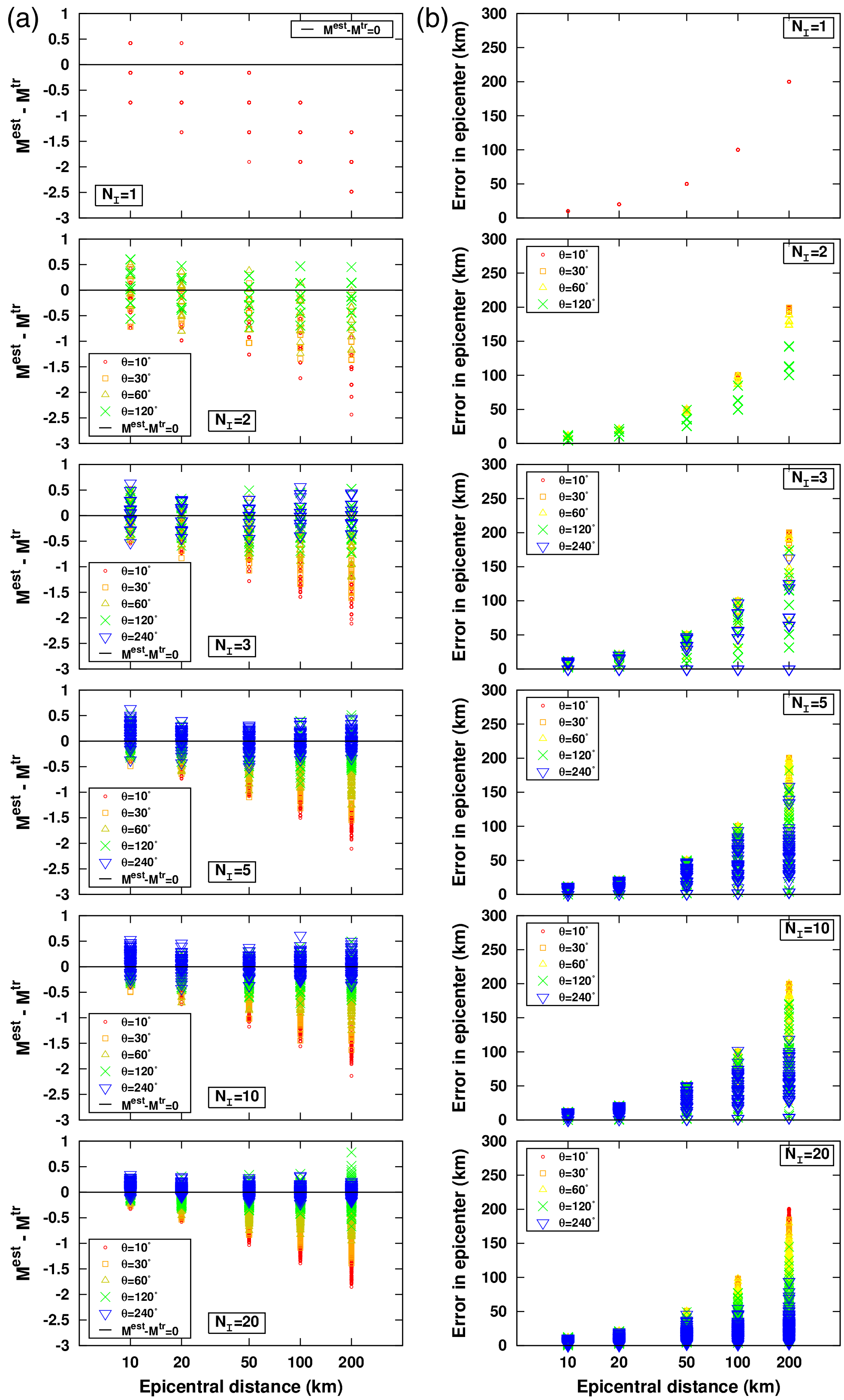

Figure 5. Variation of errors in (a) magnitudes and (b) locations as a function of epicentral distance of seismic-intensity observation point for various combinations of numbers of seismic-intensity data ($N_I = 1, 2, 3, 5, 10, 20$) and azimuthal ranges ($\theta = 10°, 30°, 60°, 120°, 240°$) in synthetic experiments. The errors generally decrease with the number of seismic-intensity data and azimuthal coverage, and increase with distance. The color version of this figure is available only in the electronic edition.

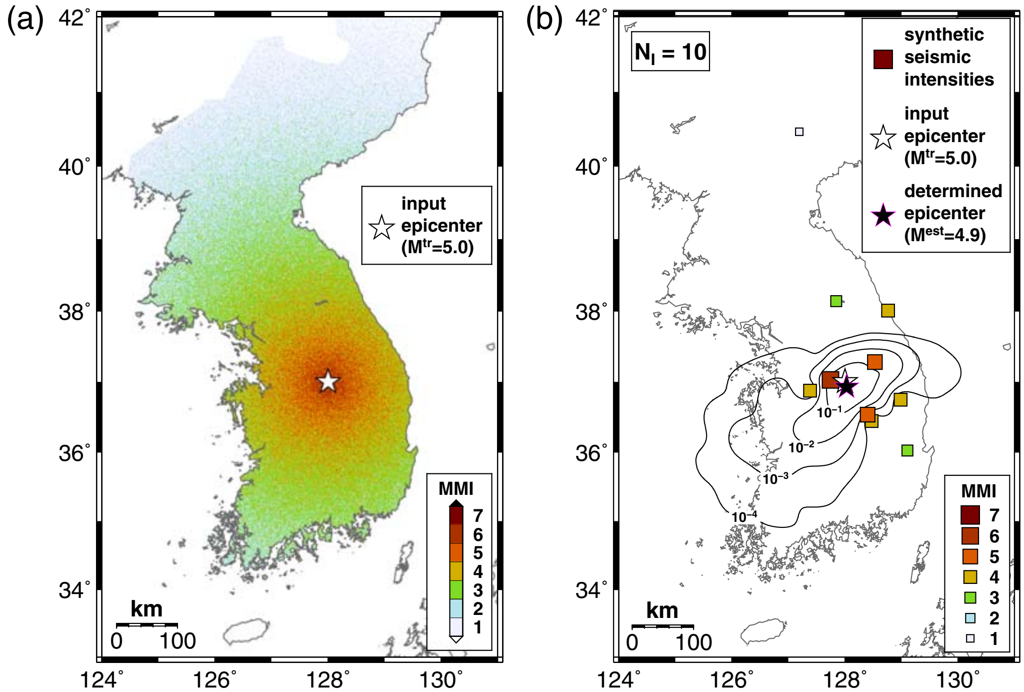

Figure 6. (a) Spatial distribution of synthetic seismic intensities for an earthquake (open star) with magnitude of $M^{tr} = 5.0$. The synthetic seismic intensities are generated by adding random noises with strength of 0.65 in modified Mercalli intensity (MMI) unit to the reference seismic intensities. (b) An example of determination of event magnitude and epicenter from an inversion based on 10 randomly selected seismic-intensity data (filled squares). The probabilities of potential locations are marked with contour lines on the map. The errors in determined magnitudes and epicenters are 0.1 in magnitude unit and 8.7 km. The color version of this figure is available only in the electronic edition.

The errors of epicenter estimates are populated around zero, suggesting reasonable determination of epicenters (Fig. 8). The 90% of epicenter estimates from the inversions based on single seismic-intensity data have the errors less than 153 km, while those from the inversions based on 2–5 seismic-intensity data display the errors less than 104–134 km. It is observed that the location errors of epicenters generally decrease with the number of seismic intensities.

It is noteworthy that the accuracy of epicenter estimates is dependent on the source environment. The magnitudes and epicenters of inland events are better determined than those of offshore events due to the azimuthal coverage of stations (Fig. 7). Also, the accuracy of inverted source parameters generally increases with the number of seismic-intensity data implemented for inversion. The offshore events naturally suffer from poor location constraints due to limited azimuthal coverage of stations and large epicentral distances. The source parameters of offshore events at large distances are poorly constrained even by the inversions based on large numbers of seismic-intensity data.

Application to Instrumental Earthquakes

The proposed method is applied to instrumentally recorded earthquakes with reported seismic intensities (Fig. 9). We analyze 55 instrumentally recorded earthquakes with magnitudes greater than or equal to 3.0 during 2001–2013. Examples of spatial distributions of seismic intensities are presented in Figure 9. The number of reported seismic intensities generally decreases with epicentral distance. The observation points of seismic intensities are populated near the epicenters for inland events (e.g., the 20 January 2007 M_L 4.8 earthquake and the 29 October 2008 M_L 3.4 earthquake), while around the coastal regions nearest to the epicenters for offshore events (e.g., the 31 May 2008 M_L 4.2 earthquake).

The epicenters and magnitudes of inland events are well determined from the inversion, while those of far offshore events are poorly constrained (Fig. 9d). Also, we observe that the errors of the inverted source parameters generally decrease with number of seismic-intensity data (Fig. 10). The errors observed in instrumental earthquakes are consistent with those observed in synthetic earthquakes, supporting the validity of the method.

Application to Historical Earthquakes

The method is applied to historical earthquakes of which source parameters were poorly constrained. Seismic damage records of two historical earthquakes are analyzed (Table 2). Seismic intensities are assigned to the seismic damage records (KMA, 2012a). The number of seismic-intensity data for the 20 July 1594 earthquake is 12, and the largest seismic intensity is determined to be MMI VIII. We also collect 11 seismic intensities varying up to MMI VI for the 2 November 1692 earthquake. The seismic intensities for the inland event (the 20 July 1594 earthquake) generally decrease with dis-

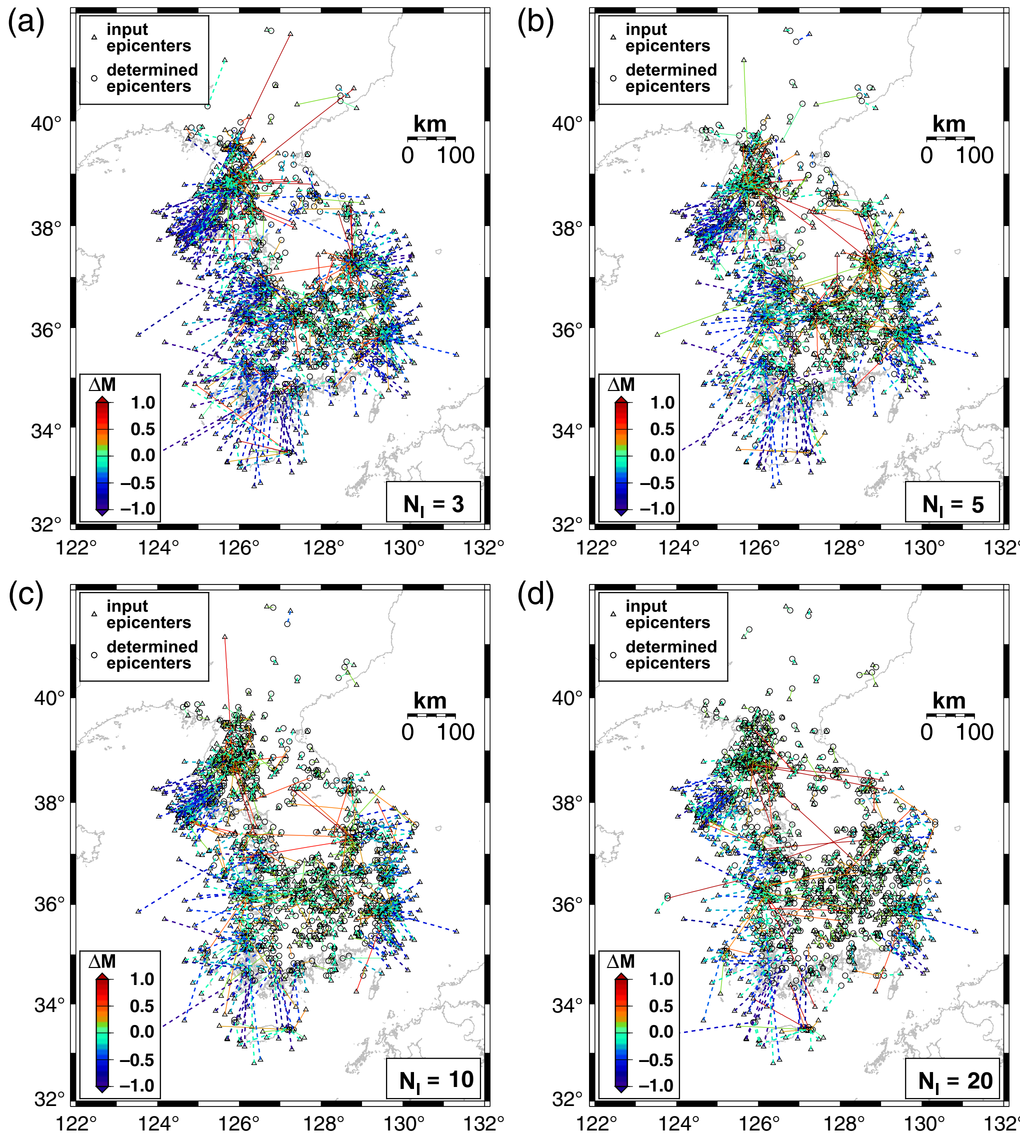

Figure 7. Determination of magnitudes and epicenters of 1000 synthetic events for inversions based on (a) 3, (b) 5, (c) 10, and (d) 20 seismic-intensity data ($N_I = 3, 5, 10, 20$). The determined locations of epicenters (open circles) are connected to the true locations (open triangles) by lines with presentation of magnitude errors (ΔM). The magnitude and location errors generally decrease with the number of seismic-intensity data. Offshore events generally display larger errors than inland events due to limited azimuthal coverage and relatively large distances to locations of seismic intensities. The color version of this figure is available only in the electronic edition.

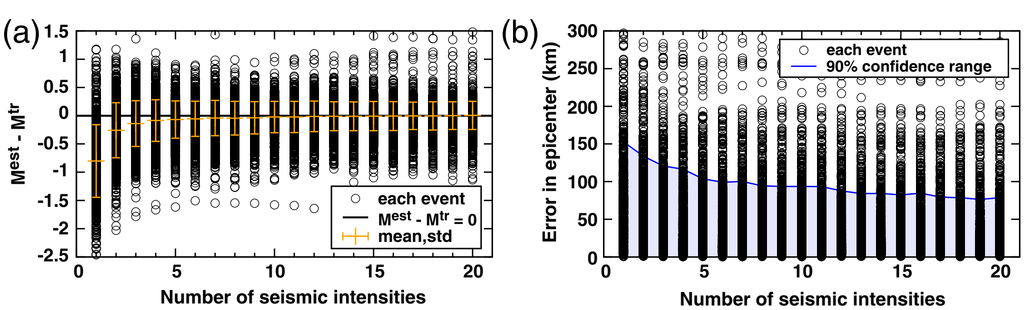

Figure 8. (a) Variation of magnitude errors ($M^{\mathrm{est}} - M^{\mathrm{tr}}$) as a function of the number of seismic-intensity data for a synthetic earthquake. The mean values and standard deviations are marked with bars. (b) Variation of location errors as a function of the number of seismic-intensity data. The 90% confidence range of the location errors is marked with a solid line. The magnitude and location errors generally decrease with the number of seismic-intensity data. The color version of this figure is available only in the electronic edition.

Table 1
Variation of Errors in Magnitudes and Epicenters with Change of the Number of Seismic-Intensity Data (N_I).

N_I	$\overline{\Delta M}$	$\sigma(\Delta M)$	$\overline{\Delta D}$ (km)	$\sigma(\Delta D)$ (km)	ΔD_{90} (km)
1	−0.80	0.64	78	99	153
2	−0.26	0.49	63	85	134
3	−0.14	0.41	56	78	121
4	−0.08	0.37	53	73	117
5	−0.07	0.33	48	69	104
6	−0.06	0.31	45	64	99
7	−0.04	0.31	44	65	100
8	−0.04	0.30	41	60	94
9	−0.04	0.29	40	59	94
10	−0.02	0.28	39	59	94
11	−0.02	0.28	39	61	93
12	−0.01	0.27	38	59	88
13	−0.01	0.26	36	56	84
14	−0.01	0.26	35	55	84
15	−0.01	0.26	35	54	82
16	−0.01	0.26	34	55	85
17	0.00	0.24	33	52	80
18	0.00	0.25	33	54	79
19	0.00	0.25	33	54	76
20	0.01	0.25	32	54	79

The mean values $\overline{\Delta M}$ and standard deviations $\sigma(\Delta M)$ of magnitude errors in magnitude unit, and the mean values $\overline{\Delta D}$ and standard deviations $\sigma(\Delta D)$ of epicenter errors in kilometers along with the 90% confidence range ΔD_{90} are presented.

tance from the site of largest damage, while those for the offshore event (the 20 July 1594 earthquake) present a weak distance-dependent feature.

The source parameters of the historical events are determined using the seismic intensities (Fig. 11). The most probable epicenter of the 20 July 1594 earthquake is determined to be (36.625° N, 126.675° E). The 90% confidence range of epicenter is a circular area with radius of 88 km from the location of peak probability, considering the error ranges in synthetic tests (Table 1). Also, the most probable magnitude is estimated to be M_{L} 5.5 with the 90% confidence range between M_{L} 5.02 and 5.94. Similarly, the most probable location of the epicenter for the 2 November 1692 earthquake is calculated to be 37.075° N and 126.075° E with the 90% confidence range of 93 km from the most probable location. The magnitude is determined to be M_{L} 4.9 with the 90% confidence range of M_{L} 4.45–5.33.

The probability is observed to decrease rapidly with distance from the most probable epicenter for the 20 July 1594 earthquake, suggesting high reliability of determined source parameters (Fig. 11). On the other hand, the offshore event (the 2 November 1692 earthquake) displays equiprobabilities over a wider region compared with the inland event (the 20 July 1594 earthquake). The source parameters determined in this study are compared with those from a previous study based on conventional approach (Lee and Yang, 2006). In conventional studies, the epicenters of historical events are determined to be the locations with the largest damages or the central locations of the equifelt areas (e.g., Lee and Yang, 2006). The epicenters of the inland event (the 20 July 1594 earthquake) are determined to be close to the location from the conventional approach. On the other hand, the epicenter of the offshore event (the 2 November 1692 earthquake) is located in a large distance away from the location from the conventional approach. This observation suggests that the proposed method can be effective for events of which seismic intensities display no apparent spatial concentration.

Discussion and Conclusions

We introduced a novel method based on seismic-intensity data to determine the event magnitude and epicenter. A set of magnitude and epicenter with the highest probability is determined for given seismic-intensity data using the seismic-intensity attenuation curve, seismicity density distribution, and Gutenberg–Richter magnitude–frequency relationship. The spatial distribution of seismicity densities and the Gutenberg–Richter magnitude–frequency relationship is assumed to be consistent with time, which may be reasonable for regions with stationary seismicity.

The validity of the method was tested with synthetic and instrumental earthquake data. It is observed that the errors of source-parameter estimates are dependent on the number, epicentral distances, and azimuthal coverage of seismic-intensity data. The errors generally decrease with increasing number and azimuthal coverage of seismic-intensity data and increase with epicentral distances. The source parameters of inland events with good azimuthal coverage are determined well. On the other hand, the offshore events suffer from limited azimuthal coverage, yielding the source-parameter estimates with relatively low accuracy. The analysis of offshore events may require additional constraints for better determination. The method was applied to two historical earthquakes, and was found to useful for determination of source parameters that had been poorly constrained. The method appears to be promising for historical earthquakes of which source properties are rarely known.

In particular, the method may be applicable to regions in which large earthquakes occur irregularly or with long recurrence intervals. There were reports on the spatiotemporal migration of large earthquakes in some intraplate regions (e.g., Liu *et al.*, 2011; Hough, 2014). The proposed method in this study may be suited for any regions with temporally stationary background seismicity. The method does not require including past large earthquakes in the reference seismicity records that is constructed based on the number of small-sized earthquakes. It was proved that the locations of past large earthquakes can be determined well based on the reference seismicity densities of small earthquakes (Houng and Hong, 2013). The observations suggest that the performance of the method may be hardly affected by the migration of large events. We expect that the proposed method may enable us to assess the seismicity properties of long periods that are crucial for assessment of potential seismic hazards.

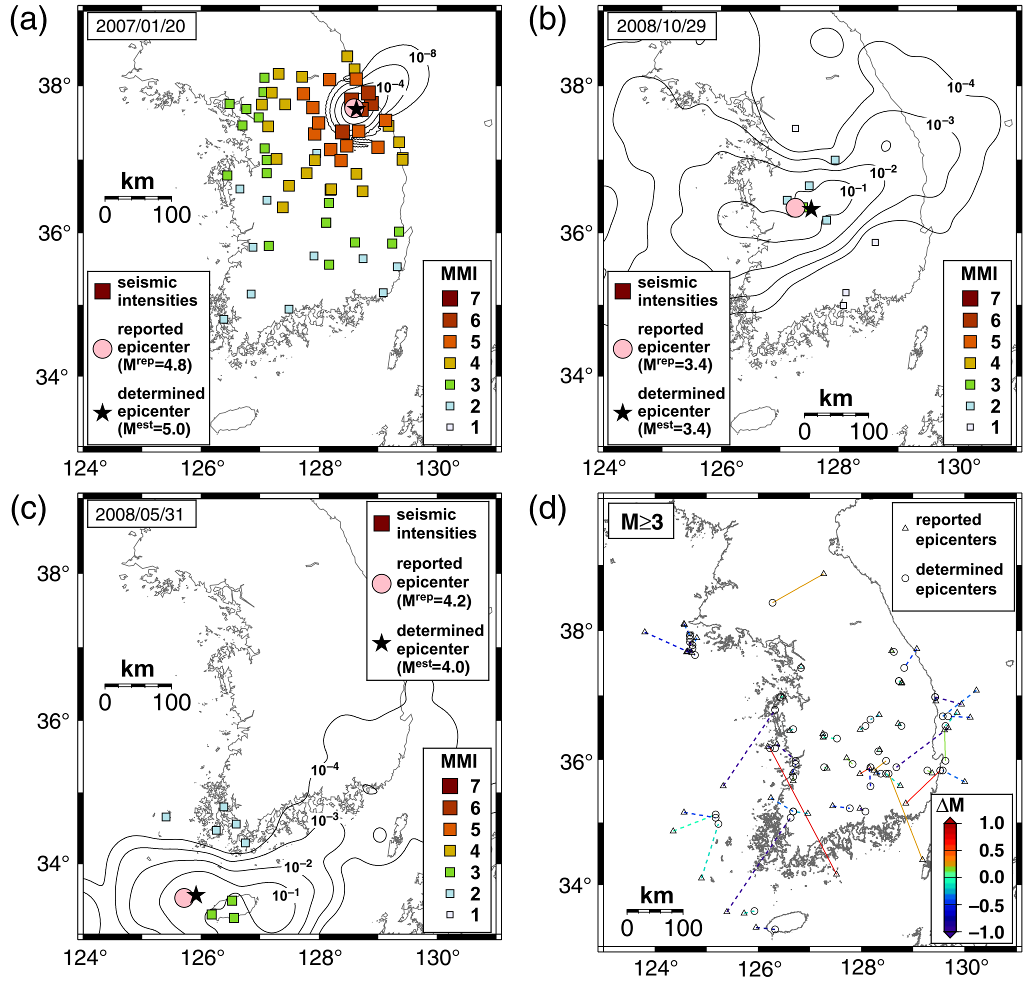

Figure 9. Determination of magnitudes and locations of three instrumentally recorded earthquakes: (a) the 20 January 2007 M_L 4.8 earthquake, (b) the 29 October 2008 M_L 3.4 earthquake, and (c) the 31 May 2008 M_L 4.2 earthquake. The seismic intensities are denoted with filled squares. The estimated magnitudes are close to the reported magnitudes, and the determined locations (filled stars) are placed near to the reported locations (filled circles). The spatial distribution of estimated probabilities is presented by contour lines. (d) The errors of estimated magnitudes and locations of all analyzed instrumentally recorded events are presented. The source parameters of inland events are determined well, while those of offshore events display large deviations. The color version of this figure is available only in the electronic edition.

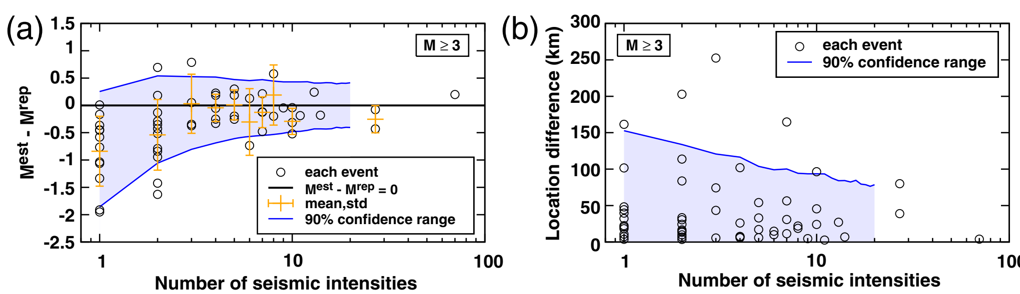

Figure 10. (a) Variation of differences between estimated and reported magnitudes ($M^{est} - M^{rep}$) as a function of the number of seismic-intensity data. The mean values and standard deviations of the differences are denoted with bars. The 90% confidence range of errors from the synthetic tests is marked with solid lines. (b) Variation of differences between estimated and reported locations as a function of the number of seismic-intensity data. The 90% confidence range of location errors from the synthetic tests is presented (solid line). The observed differences of magnitudes and locations for instrumentally observed earthquakes are consistent with those for synthetic events. The color version of this figure is available only in the electronic edition.

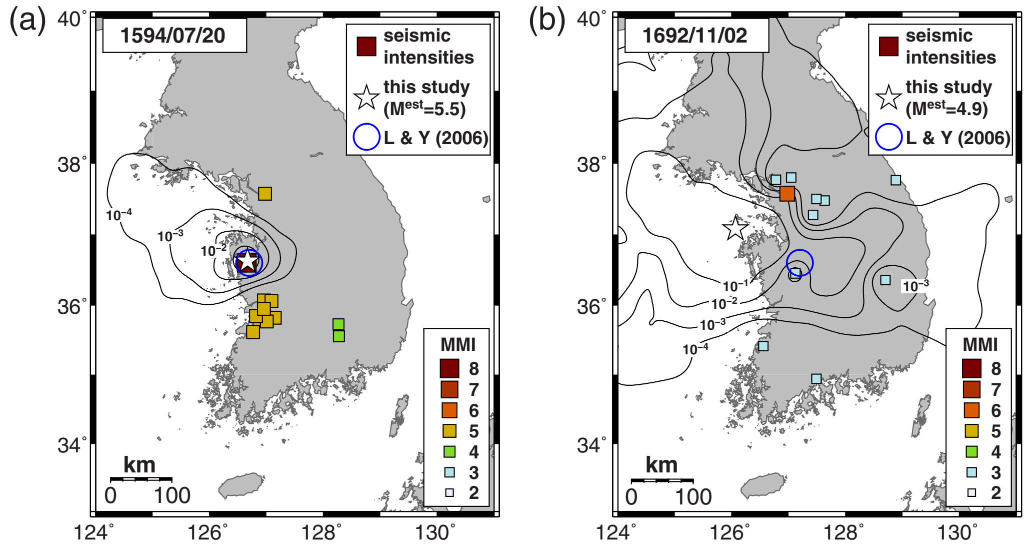

Figure 11. Determination of magnitudes and locations of two historical earthquakes: (a) the 20 July 1594 event and (b) the 2 November 1692 event. The seismic intensities for the events are denoted by squares. The magnitudes (M^{est}) are determined to be 5.5 and 4.9, respectively. The determined locations are presented by open stars. The locations of the events in a previous study (Lee and Yang, 2006) are presented for comparison (open circles). The spatial distribution of estimated probabilities is presented by contour lines. The color version of this figure is available only in the electronic edition.

Data and Resources

The Generic Mapping Tools (Wessel and Smith, 1998) were used to generate most figures. The seismic source information and waveforms were collected from the Korea Meteorological Administration (KMA) (www.kma.go.kr/weather/earthquake/report.jsp, last accessed December 2014) and the Korea Institute of Geoscience and Mineral Resources (quake.kigam.re.kr/pds/db/db.html, last accessed December). Seismic-intensity data of instrumental earthquakes were collected from KMA (2002, 2003, 2004, 2005, 2006, 2007, 2008, 2009, 2010, 2011, 2012b, 2013, 2014) and Kyung *et al.* (2007). The historical seismic damage records were collected from KMA (2012a).

Table 2
Distribution of Seismic Intensities of Two Historical Earthquakes

Date (yyyy/mm/dd)	MMI	Number of Data	Felt Place (Latitude (° N), longitude (° E))
1594/07/20	VIII	1	Hongseong (36.60°, 126.66°)
	V	9	Seoul (37.57°, 126.98°), Jeonju (35.82°, 127.15°), Gimje (35.80°, 126.88°), Gobu (35.62°, 126.77°), Yeosan (36.06°, 127.09°), Iksan (35.95°, 126.96°), Geumgu (35.77°, 127.01°), Mangyeong (35.85°, 126.82°), Hamyeol (36.07°, 126.96°)
	IV	2	Chogye (35.56°, 128.27°), Goryeong (35.73°, 128.26°)
1692/11/02	VI	1	Seoul (37.57°, 126.98°)
	III	10	Yangju (37.79°, 127.05°), Paju (37.76°, 126.78°), Icheon (37.27°, 127.43°), Jije (37.47°, 127.64°), Yangpyeong (37.49°, 127.49°), Gongju (36.45°, 127.12°), Suncheon (34.95°, 127.49°), Mujang (35.42°, 126.56°), Uiseong (36.36°, 128.69°), Gangneung (37.75°, 128.88°)

MMI, modified Mercalli intensity.

Acknowledgments

We are grateful to Associate Editors Allison Bent and Susan Hough and three anonymous reviewers for their valuable review comments that improved the presentation of the manuscript. This work was supported by the Korea Meteorological Administration Research and Development Program under Grant KMIPA 2015-7040.

References

Aki, K. (1965). Maximum-likelihood estimate of *b* in the formula log and its confidence limits, *Bull. Earthq. Res. Inst. Univ. Tokyo* **43,** 237–239.

Albarello, D., A. Berardi, C. Margottini, and M. Mucciarelli (1995). Macroseismic estimates of magnitude in Italy, *Pure Appl. Geophys.* **145,** 297–312.

Bakun, W. H., and C. M. Wentworth (1997). Estimating earthquake location and magnitude from seismic intensity data, *Bull. Seismol. Soc. Am.* **87,** 1502–1521.

Choi, H., T.-K. Hong, X. He, and C.-E. Baag (2012). Seismic evidence for reverse activation of a paleo-rifting system in the East Sea (Sea of Japan), *Tectonophysics* **572/573,** 123–133.

Chough, S. K., S.-T. Kwon, J.-H. Ree, and D. K. Choi (2000). Tectonic and sedimentary evolution of the Korean peninsula: a review and new view, *Earth Sci. Rev.* **52,** 175–235.

Degasperi, C., D. Slejko, A. Rebez, and M. Cergol (1991). Earthquakes felt in Trieste from the middle ages to the 18th century, *Tectonophysics* **193,** 53–63.

Frankel, A. (1995). Mapping seismic hazard in the central and eastern United States, *Seismol. Res. Lett.* **66,** 8–21.

Gómez Capera, A. A. (2006). Seismic hazard map for the Italian territory using macroseismic data, *Earth Sci. Res. J.* **10,** 67–90.

Gutenberg, B., and C. F. Richter (1954). *Seismicity of the Earth and Associated Phenomena*, Second Ed., Princeton University Press, Princeton, New Jersey.

Hong, T. K., and H. Choi (2012). Seismological constraints on the collision belt between the North and South China blocks in the Yellow Sea, *Tectonophysics* **570,** 102–113.

Hong, T.-K., J. Lee, and S. E. Houng (2015). Long-term evolution of intraplate seismicity in stress shadows after a megathrust, *Phys. Earth Planet. Int.* **245,** 59–70.

Hong, T.-K., S. Park, and S. E. Houng (2015). Seismotectonic properties and zonation of the far-eastern Eurasian plate around the Korean Peninsula, *Pure Appl. Geophys.*, doi: 10.1007/s00024-015-1170-2.

Hough, S. E. (2014). Intraplate seismic hazard: Evidence for distributed strain and implications for seismic hazard, in *Intraplate Earthquakes*, P. Talwani (Editor), Cambridge University Press, New York, 303–327.

Houng, S. E., and T.-K. Hong (2013). Probabilistic analysis of the Korean historical earthquake records, *Bull. Seismol. Soc. Am.* **103,** 2782–2796.

Howell, B. F., and T. R. Schultz (1975). Attenuation of modified Mercalli intensity with distance from the epicenter, *Bull. Seismol. Soc. Am.* **65,** 651–665.

Kawasumi, H. (1951). Measures of earthquake danger and expectancy of maximum intensity throughout Japan as inferred from the seismic activity in historical times, *Bull. Earthq. Res. Inst. Univ. Tokyo* **29,** 469–482.

Korea Meteorological Administration (2002). *Seismological Annual Report 2001*, Dongjin, Seoul, 5–10 (in Korean).

Korea Meteorological Administration (2003). *Seismological Annual Report 2002*, Dongjin, Seoul, 6–14 (in Korean).

Korea Meteorological Administration (2004). *Seismological Annual Report 2003*, Dongjin, Seoul, 6–17 (in Korean).

Korea Meteorological Administration (2005). *Seismological Annual Report 2004*, Dongjin, Seoul, 55–64 (in Korean).

Korea Meteorological Administration (2006). *Seismological Annual Report 2005*, Dongjin, Seoul, 4–104 (in Korean).

Korea Meteorological Administration (2007). *Seismological Annual Report 2006*, Dongjin, Seoul, 4–131 (in Korean).

Korea Meteorological Administration (2008). *Seismological Annual Report 2007*, Dongjin, Seoul, 4–73 (in Korean).

Korea Meteorological Administration (2009). *Seismological Annual Report 2008*, Dongjin, Seoul, 4–81 (in Korean).

Korea Meteorological Administration (2010). *Seismological Annual Report 2009*, Dongjin, Seoul, 4–109 (in Korean).

Korea Meteorological Administration (2011). *Seismological Annual Report 2010*, Dongjin, Seoul, 4–73 (in Korean).

Korea Meteorological Administration (2012a). *Historical Earthquake Records in Korea (2=1904)*, Yale Jeongpan, Seoul, 18–276 (in Korean).

Korea Meteorological Administration (2012b). *Seismological Annual Report 2011*, Dongjin, Seoul, 4–111 (in Korean).

Korea Meteorological Administration (2013). *Seismological Annual Report 2012*, Dongjin, Seoul, 4–119 (in Korean).

Korea Meteorological Administration (2014). *Seismological Annual Report 2013*, Dongjin, Seoul, 4–195 (in Korean).

Kossobokov, V. G., V. I. Keilis-Borok, D. L. Turcotte, and B. D. Malamud (2000). Implications of a statistical physics approach for earthquake hazard assessment and forecasting, *Pure Appl. Geophys.* **157,** 2323–2349.

Kyung, J. B., S. Y. Huh, J. Y. Do, and D. Cho (2007). Relation of intensity, fault plane solutions and fault of the January 20, 2007 Odaesan earthquake ($M_L = 4.8$), *J. Korean Earth Sci. Soc.* **28,** 202–213 (in Korean).

Lee, K., and W.-S. Yang (2006). Historical seismicity of Korea, *Bull. Seismol. Soc. Am.* **96,** 846–855.

Levret, A., J. C. Backe, and M. Cushing (1994). Atlas of macroseismic maps for French earthquakes with their principal characteristics, *Nat. Hazards* **10,** 19–46.

Liu, M., S. Stein, and H. Wang (2011). 2000 years of migrating earthquakes in North China: How earthquakes in midcontinents differ from those at plate boundaries, *Lithosphere* **3,** 128–132.

McGuire, R. K. (1995). Probabilistic seismic hazard analysis and design earthquakes: closing the loop, *Bull. Seismol. Soc. Am.* **85,** 1275–1284.

Miyazawa, M., and J. Mori (2009). Test of seismic hazard map from 500 years of recorded intensity data in Japan, *Bull. Seismol. Soc. Am.* **99,** 3140–3149.

Musson, R. M. W. (2005). Intensity attenuation in the UK, *J. Seismol.* **9,** 73–86.

Park, S., and T.-K. Hong (2014). Joint determination of event location and magnitude from historical seismic damage records, *Eos Trans. AGU* (Fall Meeting Suppl.), Abstract S11A-4332.

Pearthree, P. A., and S. S. Calvo (1987). The Santa Rita fault zone: Evidence for large magnitude earthquakes with very long recurrence intervals, basin and range province of southeastern Arizona, *Bull. Seismol. Soc. Am.* **77,** 97–116.

Schwartz, D. P., and K. J. Coppersmith (1984). Fault behavior and characteristic earthquakes: Examples from the Wasatch and San Andreas fault zones, *J. Geophys. Res.* **89,** 5681–5698.

Seo, J.-M., I.-K. Choi, and H.-M. Rhee (2010). A study of the historical earthquake catalog and Gutenberg–Richter parameter values of the Korean Peninsula, *Nuclear Eng. Technol.* **42,** 55–64.

Shimazaki, K., and T. Nakata (1980). Time-predictable recurrence model for large earthquakes, *Geophys. Res. Lett.* **7,** 279–282.

Sibol, M. S., G. A. Bollinger, and J. B. Birch (1987). Estimation of magnitudes in central and eastern North America using intensity and felt area, *Bull. Seismol. Soc. Am.* **77,** 1635–1654.

Sokolov, V. Y. (2002). Seismic intensity and Fourier acceleration spectra: Revised relationship, *Earthq. Spectra* **18,** 161–187.

Sørensen, M. B., D. Stromeyer, and G. Grünthal (2009). Attenuation of macroseismic intensity: A new relation for the Marmara Sea region, northwest Turkey, *Bull. Seismol. Soc. Am.* **99,** 538–553.

Stirling, M., and M. Petersen (2006). Comparison of the historical record of earthquake hazard with seismic-hazard models for New Zealand and the continental United States, *Bull. Seismol. Soc. Am.* **96,** 1978–1994.

Stirling, M. W., S. G. Wesnousky, and K. R. Berryman (1998). Probabilistic seismic hazard analysis of New Zealand, *New Zeal. J. Geol. Geophys.* **41,** 355–375.

Szeliga, W., S. Hough, S. Martin, and R. Bilham (2010). Intensity, magnitude, location, and attenuation in India for felt earthquakes since 1762, *Bull. Seismol. Soc. Am.* **100,** 570–584.

Termini, D., A. Teramo, and G. Arrigo (2005). A magnitude-felt area relation in the evaluation of the magnitude of historical earthquakes, *Pure Appl. Geophys.* **162,** 729–737.

Tilford, N. R., U. Chandra, D. C. Amick, R. Moran, and F. Snider (1985). Attenuation of intensities and effect of local site conditions on observed intensities during the Corinth, Greece, earthquakes of 24 and 25 February and 4 March 1981, *Bull. Seismol. Soc. Am.* **75,** 923–937.

Tinti, S., and F. Mulargia (1987). Confidence intervals of b values for grouped magnitudes, *Bull. Seismol. Soc. Am.* **77,** 2125–2134.

Vaseghi, S. V. (2001). *Advanced Digital Signal Processing and Noise Reduction*, Second Ed., John Wiley and Sons, 109–113, doi: 10.1002/0470841621.

Wang, J. (2004). Historical earthquake investigation and research in China, *Ann. Geophys.* **47,** 831–838.

Wessel, P., and W. H. F. Smith (1998). New, improved version of the Generic Mapping Tools Released, *Eos Trans. AGU* **79,** 579.

Wiemer, S., and M. Wyss (2000). Minimum magnitude of completeness in earthquake catalogs: Examples from Alaska, the Western United States, and Japan, *Bull. Seismol. Soc. Am.* **90,** 859–869.

Yonsei University
Department of Earth System Sciences
50 Yonsei-ro, Seodaemun-gu
Seoul 120-749, South Korea
tkhong@yonsei.ac.kr

Manuscript received 20 January 2016;
Published Online 22 March 2016